THE JOURNAL OF PHYSICAL CHEMISTRY A

Article

pubs.acs.org/JPCA

Two-Color Infrared Predissociation Spectroscopy of $C_6H_6^{2+}$ Isomers Using Helium Tagging

Juraj Jašík,[‡] Dieter Gerlich,[‡,†] and Jana Roithová*[,‡]

[‡]Department of Organic Chemistry, Faculty of Science, Charles University in Prague, Hlavova 2030/8, 12843 Prague 2, Czech Republic

[†]Department of Physics, University of Technology, 09107 Chemnitz, Germany

Supporting Information

ABSTRACT: Two-color IR−IR isomer selective predissociation spectra of helium-tagged $C_6H_6^{2+}$ are presented. The dications are generated via electron bombardment of either benzene or 1,3-cyclohexadiene. After mass selection they are injected into a 2.6 K cold ion trap where the presence of a dense He buffer gas not only cools them but also leads to He attachment. The ion ensemble is exposed to one or two intense IR pulses from optical parametric oscillators (OPOs) (1200−3100 cm^{-1}) before it is extracted, mass analyzed, and detected. On the basis of a comparison with theoretical predictions, the resulting spectral features allow us to separate and assign different isomers of $C_6H_6^{2+}$ dications. Compression of the ion cloud very close to the axis of the linear quadrupole trap and coaxial superposition of well-collimated laser beams results in the fragmentation of almost all helium complexes at specific wavelengths. This unique feature enables us to record fluence-dependent attenuation curves for individual absorption bands and thus determine not only absorption cross sections but also the composition of the ion mixture.

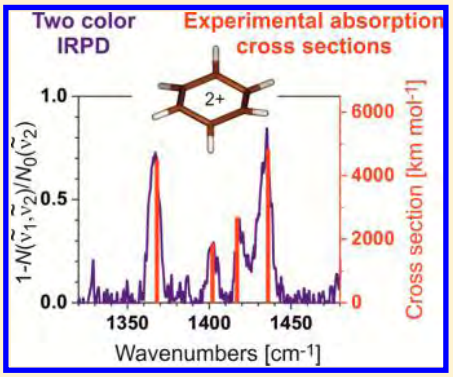

INTRODUCTION

Hydrocarbon cations are known to be prone to a variety of rearrangements.[1] Facile hydrogen atom rearrangements lead to scrambling of the hydrogen atoms within molecules, but skeletal rearrangements are also common. All of these properties are also found for doubly charged hydrocarbon cations. Hydrocarbon dications can be generated by electron ionization and the removal of two electrons usually leads to highly internally excited dications. Such dications either immediately fragment or undergo various rearrangements.[2] Experiments with partially deuterated hydrocarbon dications derived from anisole revealed that, in principle, we can expect pronounced scrambling of all hydrogen atoms within a short period of time after their generation.[3] Along with simple hydrogen-atom migrations, various skeletal rearrangements also have to be expected.[4−6]

Structural assessment of reacting dications has always been based on theoretical calculations.[4,7,8] In general, the most stable isomer of a given dication was considered to be the reactant.[9−11] To get experimental insight into the structures of dications, spectroscopic experiments are necessary. The common approach of infrared multiphoton dissociation spectroscopy for small reactive dications (such as hydrocarbon dications) has not been successful. The alternative approach of infrared predissociation spectroscopy (IRPD) relies on the use of innocent tag-atoms or tag-molecules to form loosely bound complexes.[12−17] On the basis of numerous experimental and theoretical studies, it can be assumed that in most cases a given tag does not significantly affect the structure of the studied ion.[18,19] Absorption of an IR photon triggers elimination of the tag from the complex and thus the dependence of the remaining number of loosely bound complex ions on the photon energy provides information on the IR spectrum of the studied ion.

The most common tags used in IRPD spectroscopy are argon and molecular hydrogen. These tags are not suitable for highly reactive molecular dications, because the interaction energy is rather large and we can even expect the formation of covalently bound species.[20−24] We have recently shown that IRPD spectroscopy of hydrocarbon dications can be performed with helium tagging.[25] Helium, as the smallest rare-gas atom, usually has the smallest binding energy with molecular ions and therefore also causes the smallest changes to their structures when compared to other rare-gas atoms or small molecules.[26−30]

Here, we report a full record to our recent communication on different isomers of the $C_6H_6^{2+}$ dications (Scheme 1) supplemented by experiments with two IR optical parametric oscillators (OPOs) and by recording the spectra in the fingerprint region. We have previously shown that double ionization of benzene by electron bombardment leads to a mixture of two isomers.[31] The first isomer corresponds to the

Special Issue: Markku Räsänen Festschrift

Received: August 31, 2014
Revised: November 17, 2014
Published: November 17, 2014

dx.doi.org/10.1021/jp5088064 | J. Phys. Chem. A 2015, 119, 2532−2542

Scheme 1. Isomers of $C_6H_6^{2+}$ and Their Relative Energies at 0 K Obtained at the CCSD(T)/aug-cc-pVTZ//MP2/aug-cc-pVTZ Level of Theory

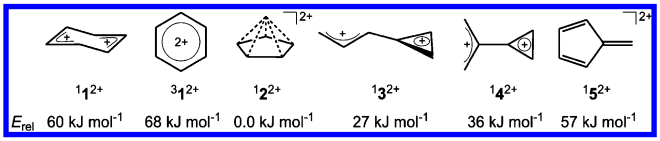

direct formation of a six-membered ring structure ($^1\mathbf{1}^{2+}$), whereas the second isomer is formed by rearrangement of the first to the more stable pyramidal structure with a five-membered base and the CH group at the apex ($^1\mathbf{2}^{2+}$).[32] The isomers were characterized by attaching helium to mass-selected ions confined in a cryogenic ion trap.[33,34] With selective photodetachment of the tag, spectra were obtained in the region of C−H stretches for both $^1[\mathbf{1}\cdot He]^{2+}$ and $^1[\mathbf{2}\cdot He]^{2+}$ complexes. With the support of calculations we have shown that the weakly bound helium atom causes only negligible alterations to the infrared spectra of the dications; so it was possible to directly compare the experimental fragmentation spectra with the theoretical IR spectra of $^1\mathbf{1}^{2+}$ and $^1\mathbf{2}^{2+}$.

EXPERIMENTAL DETAILS

The experiments were performed with the ISORI instrument.[25] ISORI is based on the combination of a low-temperature ion trap with a TSQ 7000. In its original design the commercial TSQ 7000 instrument has a quadrupole−octopole−quadrupole geometry.[35] The original vacuum chamber from the ion source is connected to the main instrument via a customized flange. It continues to serve in its original manner, with all of the options provided by the TSQ still available—here with EI source equipment. The new ultrahigh vacuum chamber consists of three additional differentially pumped regions: (1) the region with the first quadrupole ($4P_1$), the quadrupole bender (QPB), and the octopole (8P), (2) the region with the ion trap (w4PT), and (3) the second quadrupole ($4P_2$) and the detector. The ion trap has a linear quadrupole geometry where the hyperbolic shape of each electrode is approximated by six wires (more details concerning the trap and the spatial confinement of the ions can be found in ref 25 and in the Supporting Information). It is mounted into a copper box, which is screwed onto a cold-head that can reach temperatures as low as 2.6 K. Cooling of the ions is achieved by collisions with a helium buffer gas. The temperature of the box, surrounding the trap, and of the heat shield is measured by silicon-diode sensors. The buffer gas is injected by a custom-made piezo valve, situated in vacuum, directly into the trap with a straight Teflon tube. Due to condensation of He, both the increase and the decrease of the buffer-gas density are slightly delayed (Figure 1).

Timing. The timing of the experiment is illustrated in Figure 1a. For the generation of dications, we have either used benzene or 1,3-cyclohexadiene. $C_6H_6^{2+}$ ions were generated by electron ionization from the given precursor, mass-selected by the $4P_1$, deflected by the QPB, and guided by the 8P to the w4PT. Simultaneously, He buffer gas has been injected into the trap to collisionally relax the translational, rotational, and vibrational energy of the ions. As can be seen from Figure 1a, the He number density reaches a maximum of 10^{15} cm^{-3} at 10 ms, followed by a decrease with a time constant of 17 ms. The fixed and the tuned wavenumber IR OPOs (pulse length 10 ns) are fired at 74 and 75 ms, respectively. At 80 ms, the exit electrode of the trap is opened, the ions are mass-analyzed by the $4P_2$ and detected by a Daly type detector operated in ion-counting mode.

Because He is attached to $C_6H_6^{2+}$ via ternary collisions, this reaction already becomes inefficient after 30 ms and a stationary distribution of helium complexes is reached (see also Figure 1a of ref 25). The mass spectrum (Figure 1b) shows that up to six helium atoms are attached to $C_6H_6^{2+}$ with decreasing probability. We can also observe a small amount of adducts with background N_2[11] and their complexes with up to four helium atoms. Although cryopumping is very efficient, trace impurities of hydrogen, nitrogen, and oxygen are carried into the trap with the intense He pulse or pass through the trap

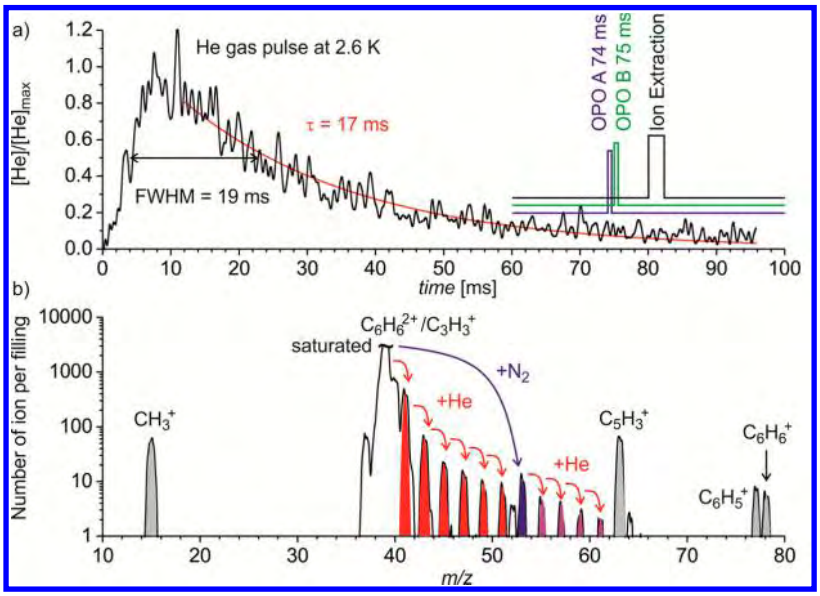

Figure 1. (a) Time sequence. The experiment is operated at the repetition rate of two synchronized Nd:YAG lasers (10 Hz). Together with a pulse of He gas, ions are injected into the trap. $[C_6H_6He_x]^{2+}$ complexes are mainly formed in the first 30 ms. At 74 and 75 ms the two IR light pulses (10 ns) interact with the ions, which are extracted at 80 ms. (b) Mass spectrum of the ions after 80 ms trapping time (without irradiation).

dx.doi.org/10.1021/jp5088064 | J. Phys. Chem. A 2015, 119, 2532−2542

as an effusive beam via the entrance and exit electrodes. It is to be noted that the $C_6H_6^{2+}$ dications are mass-selected together with the $C_3H_3^+$ monocations. For the monocations to interfere at the m/z = 41 ratio (i.e., with $[C_6H_6He]^{2+}$), their complex with an H_2 molecule would have to be formed. This has a very low probability. The IRPD spectra of $C_3H_3^+$ and $C_3H_5^+$ monocations were previously reported by Duncan and co-workers and the spectra contain different bands than those reported in the spectra.[36,37] The peaks at m/z 15 and m/z 63 indicate the preferred charge separation process of a few dications during injection of ions into the trap.

IR OPOs. To record infrared predissociation spectra of trapped $C_6H_6He^{2+}$, two identical OPO/OPA systems are available (LaserVision, tuning range 1000−4500 cm^{-1}). The OPOs are pumped by Nd:YAG lasers (Surelite EX from Continuum). Both OPO beams enter the vacuum chamber through the same CaF_2 window mounted on the detector side. The detailed preparation of the two light beams and their overlap with the stored ions are described in the Supporting Information. The energy of each IR pulse is recorded behind the exit window.

The procedure of injecting ions, cooling them, forming complexes, and triggering one or two OPOs was repeated at a frequency of 10 Hz. The number of extracted ions was usually accumulated over ten cycles. In the following ten cycles the light from the OPO was blocked by a mechanical shutter, giving the number of unirradiated ions. In one-color experiments, the number of complexes that were detected with and without irradiation are designated simply with N and N_0, respectively. If only a small number of complexes is fragmented (linear regime), the IR spectra are presented by plotting the reduced signal

$$S(\tilde{\nu}) = 1 - \frac{N}{N_0} \tag{1}$$

In the saturation regime, the plot of the remaining number of complexes, N, or the normalized ratio, N/N_0, provides more information. In most experiments with doubly charged benzene, the total number of complexes is the sum over various isomers j,

$$N = \sum_j N_j \tag{2}$$

leading to superimposed spectra.

Increasing the energy of the light pulses at a fixed wavenumber $\tilde{\nu}$ decreases the number of complexes. This measured dependence usually has been approximated with the function

$$N(E)/N_0 = A_0 + \sum_j A_j \exp(-E/E_j) \tag{3}$$

As explained below, the fitting parameters A_j are, under ideal conditions, identical to N_j. Knowing the relationship between the energy of the light pulse E and the light fluence Φ, the parameters E_j can be directly converted into the absorption cross section σ_j by making use of the identity

$$\exp(-E/E_j) = \exp(-\sigma_j\phi) \tag{4}$$

A detailed discussion as well as the used nomenclature can be found in the Supporting Information.

Two-color experiments have been performed by recording the number of ions as a function of $\tilde{\nu}_1$ while admitting the photons with the fixed wavenumber $\tilde{\nu}_2$ for 1 s and then blocking them for the next 1 s. The resulting number of ions is designated $N(\tilde{\nu}_1,\tilde{\nu}_2)$ whereas $N_0(\tilde{\nu}_2)$ is the number of complexes with the scanned OPO blocked. Such spectra are also presented by plotting the reduced signal

$$S(\tilde{\nu}_1) = 1 - \frac{N(\tilde{\nu}_1) - N(\tilde{\nu}_1,\tilde{\nu}_2)}{N_0 - N_0(\tilde{\nu}_2)} \tag{5}$$

High Fluence and Power Density, Typical Spectra. A detailed description of the spatial extensions of the ion cloud and the light beam and their mutual overlap is given in the Supporting Information. The main result is that the geometry of the light beam, the well-localized ion cloud, and their overlap can be accounted for using just 1 mm^2 as effective area of the photon beam. For the 1500 cm^{-1} range, the situation is slightly different. The photon-beam area is larger (about 3 mm^2), and the pulse energy is less than 2 mJ. With a pulse energy of 20 mJ (at 3000 cm^{-1}) one obtains a fluence of 3.4×10^{19} photons/cm^2. Due to this very high value, IR fragmentation signals can be significantly saturated. For example, complexes of dications generated from 1,3-cyclohexadiene were depleted more than 99% by irradiation at the 3089 cm^{-1} band (see below). Another important factor to consider is the rather high power density of the light beam inside the trap. Accounting for the pulse length of 10 ns, the ions are exposed to a power density of 2×10^8 W/cm^2. This can lead to various nonlinear effects such as the excitation of combination bands, two-photon processes, and also near-resonant Raman heating of the complexes without fragmentation as discussed below. The situation will certainly become more complicated if the stored ions are exposed to both lasers at the same time. So far, we have separated them by 1 ms (Figure 1).

The dependence of the resulting spectra on the light pulse energy is illustrated in Figure 2. We have recorded the spectral region of C−H stretches using a pulse energy of 1.2 mJ (lower trace) and 12 mJ (upper trace). Due to the limited number of

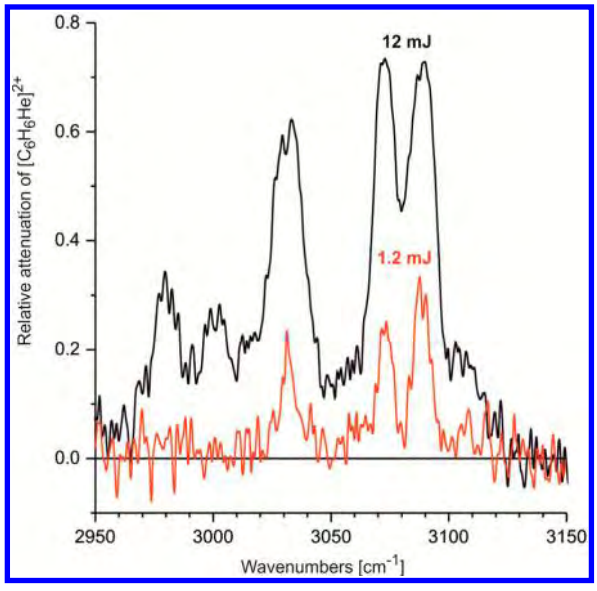

Figure 2. Relative number of fragmented complexes at the two indicated pulse energies of the IR light. With the 10 times more intense pulse, the lines are significantly saturated and power broadened. The two lines at the left do not show up with 1.2 mJ and are assigned as combination bands.

dx.doi.org/10.1021/jp5088064 | J. Phys. Chem. A 2015, 119, 2532−2542

complex ions stored in the trap, with the present arrangement it is possible to fragment all of those complexes that absorb photons with a sufficiently large cross section. Comparison reveals that the lines recorded with the high energy are significantly broadened and that the peaks are saturated because 80% of the *total number* of trapped complexes are fragmented. Another characteristic of the saturated spectrum is the occurrence of combination and overtone bands that are enhanced when the higher photon flux is used to probe the C−H stretching region. Especially evident are the two lines at 2980 and 3000 cm^{-1}, which are not observed using 1.2 mJ pulses. The very small cross sections of those bands (see below) are a clear hint that, in this spectral range, photons are absorbed via combination or overtone bands.

More quantitative information on photoinduced fragmentation can be obtained by recording the number of $[C_6H_6He]^{2+}$ complexes as a function of the pulse energy at a fixed wavelength. Figure 3a shows results recorded at 3067 cm^{-1}. At

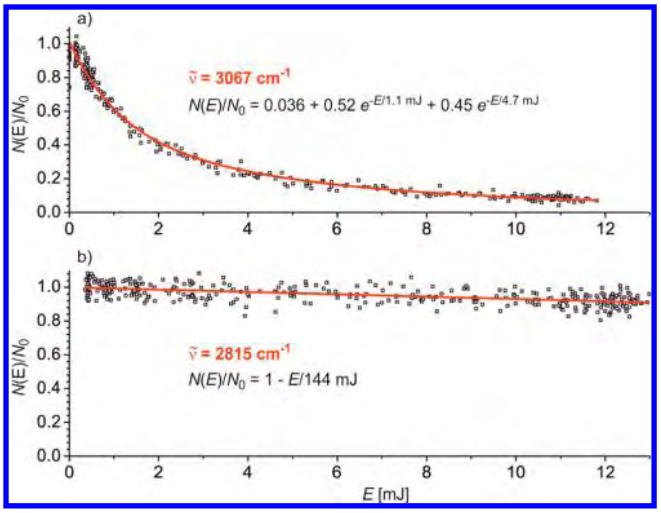

Figure 3. Dependence of the number of $[C_6H_6He]^{2+}$ complexes on the pulse energy of the photon beam. (a) At 3067 cm^{-1}, the data points decrease steeply with increasing energy. An unbiased fit reveals two exponentials and a shifted zero line. The parameters are given in the figure. (b) At 2815 cm^{-1}, a very slow decay has been observed. The resulting very small absorption cross section (Table 1) is a strong hint that, at this wavelength, absorption occurs via a combination or overtone band.

this wavelength almost all complexes are destroyed above 10 mJ. Fitting the data with eq 3 results in two characteristic energies E_1 = 1.1 mJ and E_2 = 4.7 mJ and the unaffected ions make up only 3.6%. The two pre-exponential factors, 52% and 45%, can be interpreted as two classes of ions; however, it is not obvious (see below) that this coincides with different isomers because the photon wavenumbers average over 3 cm^{-1}. Figure 3b shows the same type of measurement recorded at 2815 cm^{-1}, which is a very weak absorption feature. The attenuation is so small that it can be fitted with a linear function.[38,39]

COMPUTATIONAL DETAILS

The calculations were performed using the perturbation theory method MP2[40−42] and the density functional theory method PBEhPBE[43,44] together with the aug-cc-pVTZ basis set as implemented in the Gaussian 09 suite.[45] Computation of the Hessian matrix was performed for all optimized structures at the same level of theory to ensure that the structures correspond to genuine minima as well as to calculate the thermochemical data and IR spectra. The final energies were determined by single-point calculations at the CCSD(T)/aug-cc-pVTZ level.[46−48] It was shown in our previous communication that CCSD, MP2, M06-2X, and PBEhPBE levels of theory lead to very similar geometries for all optimized dications and that the theoretical IR spectra are also very similar at all of these levels of theory. Here, we use results obtained at the PBEhPBE level of theory as they provide the best match in the fingerprint region. Results obtained at other levels of theory can be found in the Supporting Information.

RESULTS AND DISCUSSION

As mentioned in the Introduction, electron ionization of benzene with 70 eV electrons leads to (among others) a mixture of isomeric $C_6H_6^{2+}$ dications. Using helium tagging and infrared predissociation (IRPD) spectroscopy in the C−H stretching region, we could show that this production scheme together with the transfer to the trap and the cooling process leads to a mixture of two isomers, $^1\mathbf{1}^{2+}$ and $^1\mathbf{2}^{2+}$.[31] All experimental observations and interpretations have been corroborated by the above-mentioned calculations. It has been very helpful in these experiments that we could dissociate the $^1[\mathbf{1}\cdot He]^{2+}$ complexes using a high-power CO_2 laser. Originally, we hoped that we could anneal all of the stored ions to the lowest isomer via several sequences of heating above the barriers and cooling. However, accidentally, the $^1[\mathbf{1}\cdot He]^{2+}$ isomer has infrared transitions in the range of photons emitted by this type of laser whereas the other isomer does not. Therefore, a pure IRPD spectrum of the remaining $^1\mathbf{2}^{2+}$ complexes could be recorded. This fortuitous two-color experiment will be complemented by using two independent tunable OPO/OPA systems for the generation of IR photons. In addition, the frequency range of one of the OPO/OPA systems has been extended into the C−C fingerprint region. The OPO systems now provide higher photon fluence in the trap and, as described above and in the Supporting Information, the overlap with the narrow ion cloud has been improved.

There are many two-color or double-resonance experiments that also make use of the coherence of the two light fields. Typical examples include hole-burning in molecular jets,[49] extracting ions from a trap into a TOF mass spectrometer where they can be exposed to lasers at different locations,[50,51] or IR depletion spectroscopy using VUV fragmentation.[52] In the last of the mentioned experiments, the lasers interact with ions inside a trap like in ours. In the present work it is new that the ions are squeezed into a well-collimated laser beam, leading to much higher light fluence and extreme power densities.

Figure 4a shows the IRPD spectrum of the $C_6H_6^{2+}$ dications generated by EI from benzene, now also including the fingerprint region. Comparison of the whole spectrum with theoretically determined IR spectra of various $C_6H_6^{2+}$ isomers shows a match at higher wavenumbers, if a mixture of $^1\mathbf{1}^{2+}$ and $^1\mathbf{2}^{2+}$ is considered (Figure 4b−g). The broad peak at about 2940 cm^{-1} represents a contribution from helium complexes of the $^1\mathbf{1}^{2+}$ isomer. We have shown that there is another band at about 3070 cm^{-1} originating from these ions, but it is overlapping with bands belonging to the $^1\mathbf{2}^{2+}$ dications. The pyramidal dications are represented by several overlapping peaks at 3040 cm^{-1} and at about 3070 cm^{-1}. The higher fluence (or the higher power density in the case of nonlinear transitions) of the photon beam leads to additional peaks that were not observed in the previous experiments (peaks at

dx.doi.org/10.1021/jp5088064 | J. Phys. Chem. A 2015, 119, 2532−2542

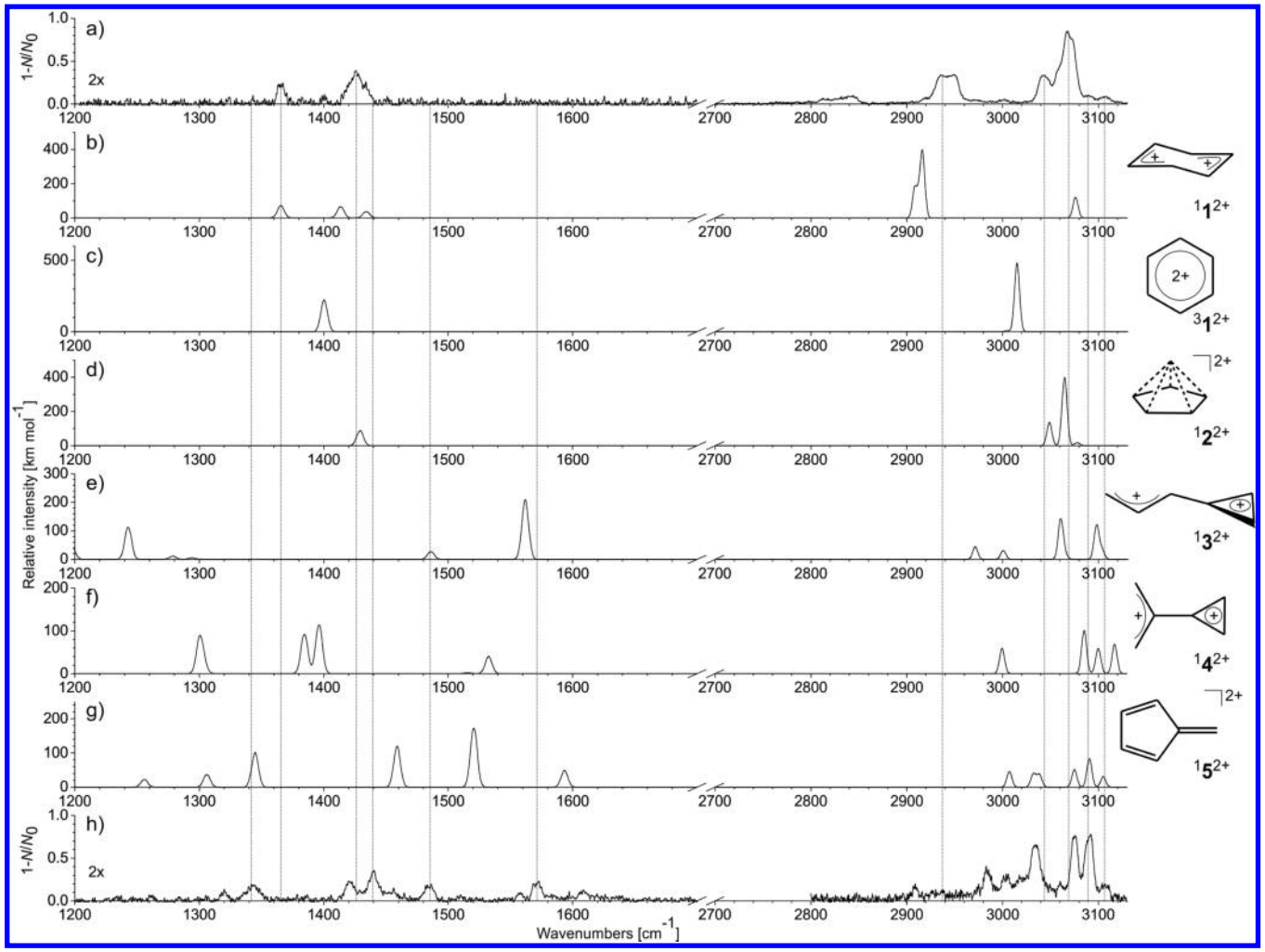

Figure 4. Helium tagging IRPD spectra of the $C_6H_6^{2+}$ dications generated by (a) double ionization of benzene and (h) dissociative double ionization of 1,3-cyclohexadiene. Note that the spectra in the fingerprint region are twice enhanced. (b)−(g) Theoretical IR spectra of different $C_6H_6^{2+}$ isomers obtained with the density functional theory model BPE, the scaling factor above 2700 cm^{-1} was 0.985 and below 2700 cm^{-1} was 1.015.

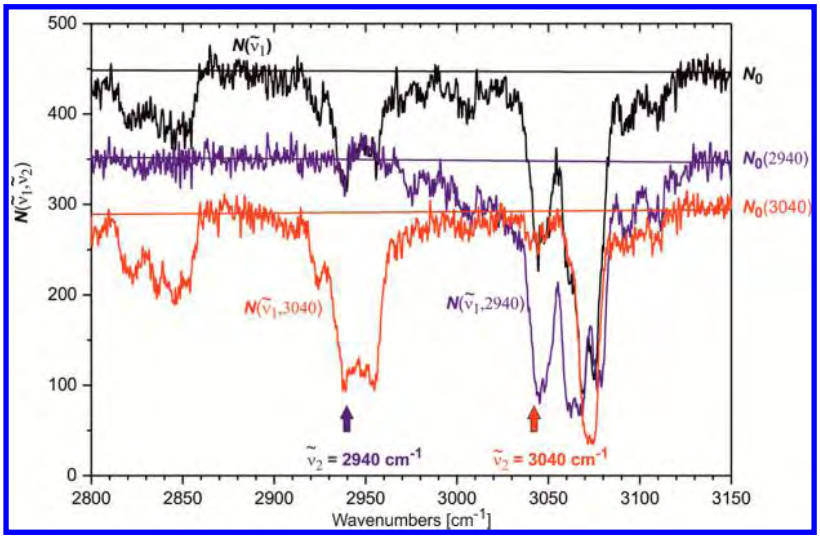

Figure 5. Two-color fragmentation of helium tagged $C_6H_6^{2+}$ dications generated from benzene. The uppermost curve shows the number of ions after being exposed only to OPO_A, which is scanned (black line). Addition of IR radiation from OPO_B at a fixed wavenumber (2940 cm^{-1} blue line, 3040 cm^{-1} red line) reduces the number of ions, as can be seen from the shifted N_0 lines. A detailed inspection reveals that some lines disappear, e.g., the combination band and the 2940 cm^{-1} feature in the blue spectrum or the 3040 cm^{-1} line in the red spectrum. It is also important to realize that the combination of both OPOs leads to additional absorption at certain wavenumbers (e.g., at 3070 cm^{-1}).

dx.doi.org/10.1021/jp5088064 | J. Phys. Chem. A 2015, 119, 2532−2542

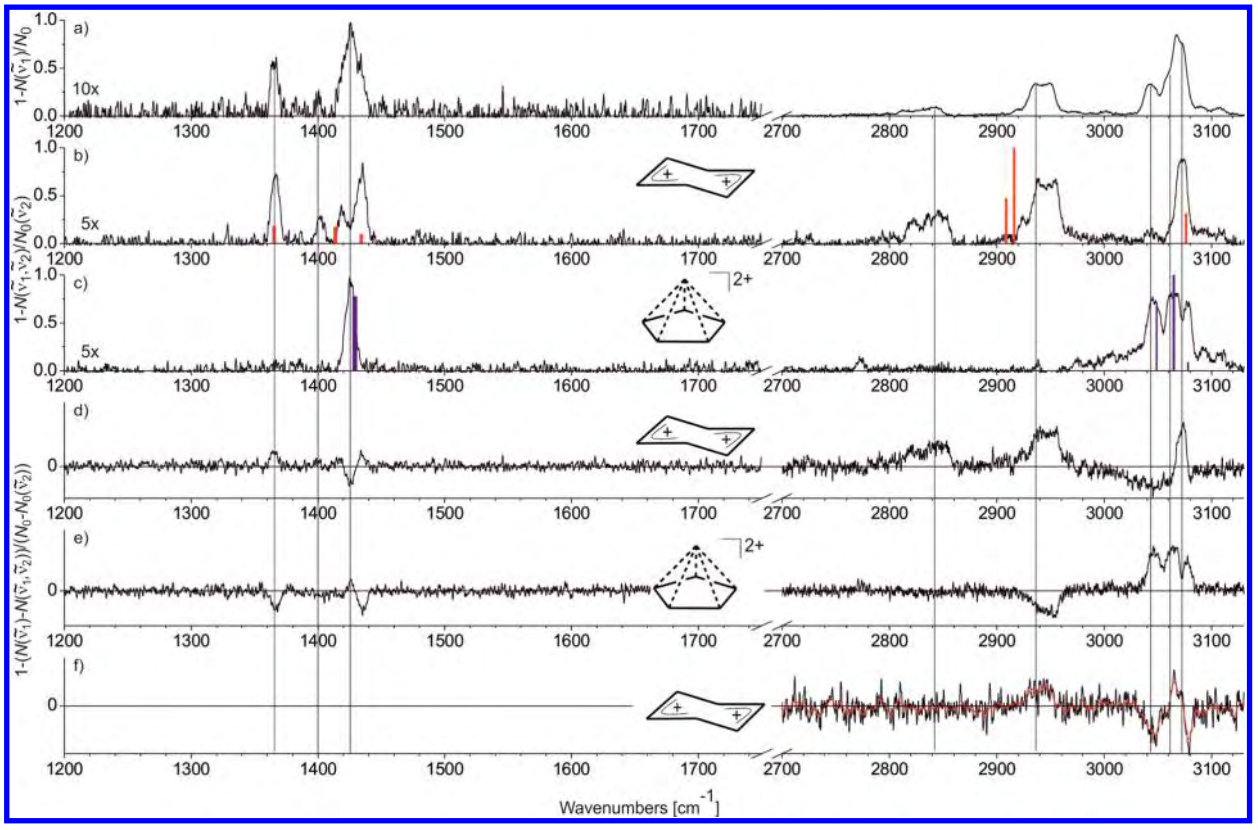

Figure 6. (a) IRPD spectrum of the helium tagged $C_6H_6^{2+}$ dications generated from benzene. Two-color IRPD spectra obtained with one OPO fixed at (b) 3040 cm^{-1} or (c) 2940 cm^{-1}. Two-color IRPD obtained according to eq 5 with the fixed OPO at (d) 2940 cm^{-1}, (e) 3040 cm^{-1}, and (f) 1400 cm^{-1}. The bar spectra indicate theoretical IR transitions of the $C_6H_6^{2+}$ isomers (the spectra above and below 2000 cm^{-1} are normalized to 1, the correct intensities can be found in Figure 4).

3090 and 3107 cm^{-1}, and a composite band at 2800−2850 cm^{-1}). The bands in the fingerprint region might also be explained by the combined contributions of $^1\mathbf{1}^{2+}$ and $^1\mathbf{2}^{2+}$, but without further analysis a contribution from other isomers of the $C_6H_6^{2+}$ dications cannot be excluded. To link the bands in the C−H stretching region (above 2700 cm^{-1}) with the C−C stretching bands and C−C−H deformation bands in the fingerprint region, we performed two-color experiments.

Two-Color IRPD Experiments. A two-color IR−IR photodissociation experiment is based on the measurement of a conventional IRPD spectrum with a scanning OPO while irradiating the ions with a second OPO set at a fixed photon energy corresponding to a certain absorption band. Photo-irradiation by the fixed OPO, which is fired 1 ms before the other in the present experiment, reduces the population of one isomer. This is demonstrated in the resulting spectrum by a relative decrease in the intensities of all bands belonging to this particular isomer. In the extreme example, when all these isomers are depleted by the fixed OPO, the measured spectrum contains only peaks belonging to the remaining isomers.

The situation where we were able to destroy almost all helium complexes of a given kind, is shown in Figure 5 (for the notations see the Experimental Details). The black line shows the remaining number of ions after irradiation by the scanned OPO $N(\tilde{\nu}_1)$ ($\tilde{\nu}_1$ refers to the scanning OPO). The $[1 - N(\tilde{\nu}_1)/N_0]$ quantity, where N_0 is the total number of the helium-tagged ions in the ion trap before irradiation gives the IRPD spectrum shown in Figure 6a. The blue line in Figure 5 shows the effect of additional irradiation on the ions at the fixed wavenumber $\tilde{\nu}_2$ = 2940 cm^{-1} ($\tilde{\nu}_2$ refers to the fixed OPO). Clearly, by irradiation of the ions at 2940 cm^{-1} we had depleted almost all of the helium complexes absorbing at this wavenumber (i.e., $^1[\mathbf{1}\cdot\mathrm{He}]^{2+}$). We can thus expect that additional depletion of the helium complexes by the scanned OPO irradiation is caused mostly by the absorption of photons by isomers other than those absorbing at $\tilde{\nu}_2$. This spectrum (blue line) is dominated by the contribution of the $^1[\mathbf{2}\cdot\mathrm{He}]^{2+}$ isomer and the normalized spectrum ($[1- N(\tilde{\nu}_1,\tilde{\nu}_2)/N_0(\tilde{\nu}_2)]$) is shown in Figure 6c (see analysis below).

The same experiment was conducted with the fixed OPO set to $\tilde{\nu}_2$ = 3040 cm^{-1} (red line). Again, the dominant part of the helium complexes absorbing at this wavenumber (i.e., $^1[\mathbf{2}\cdot\mathrm{He}]^{2+}$) was fragmented by the fixed photon-wavenumber beam (note that there is still a small population of these complexes that survive irradiation by the fixed OPO but fragment upon irradiation by the scanned OPO at the same wavenumber). The resulting red spectrum is dominated by fragmentation of helium complexes that are different from those absorbing at 3040 cm^{-1}; hence, it corresponds to the spectrum of the $^1[\mathbf{1}\cdot\mathrm{He}]^{2+}$ isomer and the normalized spectrum is shown in Figure 6b. In addition to the bands at 2940 and 3070 cm^{-1}, which were previously observed, we can identify several peaks in the 2800−2850 cm^{-1} range. These transitions are associated with the high power density of the photon beam and must correspond to overtones or combination bands. The small peaks at 3090 and 3110 cm^{-1} probably originate from an impurity (see the Supporting Information).

The two-color experiments with $\tilde{\nu}_2$ = 3040 cm^{-1} and $\tilde{\nu}_2$ = 2940 cm^{-1} were also used to separate the IRPD spectra of the individual isomeric complexes in the fingerprint region. The

dx.doi.org/10.1021/jp5088064 | J. Phys. Chem. A 2015, 119, 2532−2542

normalized spectra are shown in Figures 6b and 6c, respectively. The spectrum corresponding to the $^1[\mathbf{1}\cdot He]^{2+}$ complexes contains four bands in the fingerprint region (Figure 6b). Theoretically, only three peaks would be expected in the spectrum of $^1\mathbf{1}^{2+}$, but we have to take into account that coordination of helium to different positions of the six-membered ring may lead to shifts in the band positions and result in more complicated spectra. For the pyramidal $^1[\mathbf{2}\cdot He]^{2+}$ complexes (Figure 6c) only one band at 1427 cm^{-1} is detected, which is in agreement with theory. This band corresponds to the C−C stretch in the five-membered ring at the base of the $^1\mathbf{2}^{2+}$ pyramid.

The presented straightforward evaluation of the spectra in the two-color experiments was only possible because of the fortunate situation of having only two isomeric complexes and being able to significantly reduce the population of each of the isomers. This is certainly not a normal situation. The alternative approach for the evaluation of the two-color IRPD data obtained from our experiments is based on the separation of the changes introduced by the irradiation by the fixed OPO on the IRPD spectrum obtained by the scanned OPO. Application of eq 5 to the results obtained for irradiation of the $^1\mathbf{1}^{2+}$ isomers at 2940 cm^{-1} and the $^1\mathbf{2}^{2+}$ isomers at 3040 cm^{-1} leads the spectra shown in Figure 6d,e, respectively. Clearly, we can see peaks corresponding to the $^1\mathbf{1}^{2+}$ isomer and the $^1\mathbf{2}^{2+}$ isomer, respectively. We have also detected negative peaks in both spectra. We will return to their explanation later.

To test the evaluation according to eq 5, we have measured a two-color IRPD spectrum with the fixed OPO at 1400 cm^{-1} while scanning the region of the C−H stretches (Figure 6f). We have selected this peak because it could potentially represent a contribution of the triplet state dication $^3\mathbf{1}^{2+}$. Although the relative changes in the IRPD spectrum imposed by irradiation at 1400 cm^{-1} are very small, it is still evident that this peak belongs to the singlet state dication $^1\mathbf{1}^{2+}$. This experiment was done to prove or disprove any possible involvement of the triplet state of the benzene dication ($^3\mathbf{1}^{2+}$). The transition at 1400 cm^{-1} fits very well with the theoretical prediction of the IR spectrum of $^3\mathbf{1}^{2+}$, and it could be possible that the stretching vibration of the C−H bonds predicted at 3015 cm^{-1} could be shifted and thus overlapped by the bands of dominant isomers $^1\mathbf{1}^{2+}$ and $^1\mathbf{2}^{2+}$. Nevertheless, this scenario does not appear to be correct. See also below the power-dependence measurements, which show that all four bands assigned to the $^1\mathbf{1}^{2+}$ isomer belong to only one group of ions.

Synergic Effects in Two-Color IRPD Spectra. The negative peaks in the spectra shown in Figures 6d−f are the result of increased fragmentation of ions that are off-resonance being irradiated by the second OPO. This effect can be observed in Figure 5 (compare black and red lines): Irradiation of the ion cloud by the fixed OPO at 3040 cm^{-1} not only leads to fragmentation of the $^1[\mathbf{2}\cdot He]^{2+}$ complexes absorbing at this wavenumber but also secondarily leads to an enhancement of the fragmentation of the $^1[\mathbf{1}\cdot He]^{2+}$ complexes induced by the scanning OPO at 2940 cm^{-1}. By sole irradiation at 2940 cm^{-1}, about 100 helium complexes are fragmented (out of 450). If the ions are first irradiated at 3040 cm^{-1} and afterward probed by irradiation at 2940 cm^{-1}, the number of the depleted $^1[\mathbf{1}\cdot He]^{2+}$ complexes approximately doubles. The same effect was observed if the order of the OPO shots was reversed. The extent of the fragmentation enhancement slightly depended on the time interval between the two OPO pulses, but it was always present. The reason for this effect is not clear, but we speculate about the possibility of preheating the complexes via inelastic photon scattering or excitation of some combination bands or overtones accidently present in the wavenumber range considered as being off-resonance.

Quantitative Measurements. We have again demonstrated that upon electron ionization of benzene a mixture of $^1\mathbf{1}^{2+}$ and $^1\mathbf{2}^{2+}$ isomers is formed. The second step in the analysis of this mixture is to determine how many dications of each isomer are really present in the trap. Certainly, the relative abundance of the isomers can be slightly modified by the conditions in the ion source. Presumably, the initially hot ions decay at different rates either by fragmentation reactions or by reactions with impurities in the ion source. The dications may also undergo isomerization reactions in collisions with helium when they are injected into the trap, and the ternary rate coefficients for forming the $[C_6H_6He]^{2+}$ complexes may depend on the structure of the dication. Nevertheless, after relaxation to the low temperature of the trap, it is rather unlikely that the isomers lying higher in energy would relax to the more stable ones, because the energy barriers for the rearrangement are too high (about 1 eV).[31] We can thus assume that under given experimental conditions, we are working with a given mixture of isomers and we should be able to determine their representation.

In the quantitative analysis of the isomers in the mixture, we have taken advantage of the high photon fluence that the complexes are exposed to. Figure 7 shows the total numbers of the $[C_6H_6He]^{2+}$ complexes as a function of the photon energy E at selected wavenumbers. The measured attenuation curves have been simply fitted with a single exponential curve (eq 3). The number A_0 summarizes all the $[C_6H_6He]^{2+}$ complexes that are not affected by the irradiation at the given wavenumber. This may be due to no absorption at the given wavenumber, or the fact that a few complexes might be outside of the photon beam (distortions of the dc part of the trapping potential). The possibility of isobaric impurities such as $[C_3H_5]^+$ ($C_3H_3^+$ and $C_6H_6^{2+}$ ions have the same m/z ratio and are thus both injected into the ion trap, H_2 is present in the background of the ion trap) should be also taken into account.

Figure 7 show relative attenuation curves and their fits for the band at 3040 cm^{-1} (Figure 7a) and all the detected bands in the fingerprint regions (Figures 7b-f). For these experiments, the beam splitter for the merging of the photon beams was removed, so we achieved much larger power densities including in the fingerprint region compared to those achieved during measurements of the spectra reported in Figure 6. The fits were obtained under the constraint that we are dealing with 40% of isomer $^1\mathbf{1}^{2+}$, 40% of isomer $^1\mathbf{2}^{2+}$, and 20% of a background (which may be singly charged ions or other impurities). The fits provide characteristic constants E_i that were converted to absorption coefficients (Table 1).[53]

The spectra for the C−H stretching region were measured at clearly nonlinear absorption conditions, but the spectra determined in the fingerprint region were measured with a much lower light fluence and therefore the relative peak intensities should be proportional to the absorption cross sections of the individual group of ions. Figure 8 shows a comparison of the spectrum measured for the $^1\mathbf{1}^{2+}$ dications in a two-color IR−IR experiment (see above Figure 6) and the absorption cross sections determined for the individual bands in the attenuation experiments. Undoubtedly, both results give a consistent picture.

dx.doi.org/10.1021/jp5088064 | J. Phys. Chem. A 2015, 119, 2532−2542

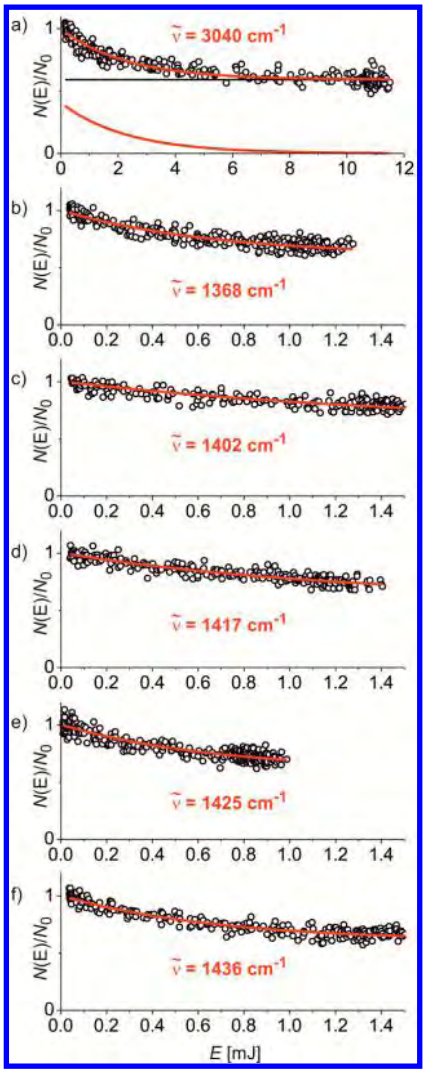

Figure 7. Attenuation measurements at the indicated wavelengths (a)−(f). Constrained fitting of the data reveals that 40% of the ions must be $^1\mathbf{1}^{2+}$ isomers, and 40% $^1\mathbf{2}^{2+}$ isomers. The remaining 20% are either other isomers or other ions on m/z = 41, which do not absorb the photons at the tested wavelengths. The resulting characteristic energies E_j and therefore the absorption cross sections differ significantly (Table 1).

Other $C_6H_6^{2+}$ Isomers. After demonstrating the power of the two-color IRPD approach for determination of the isomeric mixtures of ions, we extended our study to other isomers of $C_6H_6^{2+}$. The question in many conventional reactivity studies of hydrocarbon dications is whether it is acceptable to assume that the ions are mostly present in their most stable structures. For example, we have shown that all $C_7H_6^{2+}$ dications generated by dissociative double ionization from toluene rearrange to the most stable cycloheptatrienylidene isomer, although several structures with a six-membered ring can be formed.[25] In analogy, here we have investigated, whether $C_6H_6^{2+}$ dications generated by dissociative ionization of 1,3-cyclohexadiene also mostly isomerize to the most stable $^1\mathbf{2}^{2+}$ isomers. Double ionization of 1,3-cyclohexadiene in fact leads to doubly protonated benzene and the dominant fragmentation of these dications is dehydrogenation leading to the required $C_6H_6^{2+}$ dications.[54]

The IRPD spectrum of these dications clearly differs from the spectrum of the dications generated from benzene (cf. Figure 4a,h). The straightforward answer to the posed question is thus "no, it should not be expected that we are dominantly generating the most stable isomers of a given hydrocarbon dication". The assignment of the structure of the $C_6H_6^{2+}$ ions generated from 1,3-cyclohexadiene is not obvious on the basis of comparison with theory. We have therefore again applied two-color IR-IR photodissociation spectroscopy.

We note in passing that we have also checked the IRPD spectrum of $C_6H_6^{2+}$ dications generated by dissociative ionization of 1,4-cyclohexadiene. It was suggested that double ionization of 1,3-cyclohexadiene leads to the singlet state of doubly protonated benzene and the double ionization of 1,4-cyclohexadiene yields a mixture of the singlet and triplet states of doubly protonated benzene.[54] Nevertheless, the IRPD spectra of the helium complexes of $C_6H_6^{2+}$ generated either from 1,3-cyclohexadiene or from 1,4-cyclohexadiene were identical within the experimental uncertainty.

We have measured two-color IRPD spectra corresponding to the IRPD spectrum shown in Figure 9a with the fixed OPO tuned to every peak detected above 2900 cm^{-1}. Most of the spectra, however, were almost identical to the one-dimensional

Table 1. Photoinduced Fragmentation Cross Sections Estimated from the Characteristic Energies at Different Wavenumbers for the $C_6H_6^{2+}$ Dications Generated from Benzene and 1,3-Cyclohexadiene[a]

$\tilde{\nu}$ [cm^{-1}]	E_j [mJ]	σ^b [cm^2]	σ^b [km mol^{-1}]
	$C_6H_6^{2+}$ Generated from Benzene		
1368	0.67	1.2 × 10^{-18}	4499
1402	1.72	4.9 × 10^{-19}	1841
1417	1.20	7.0 × 10^{-19}	2695
1425	0.67	1.3 × 10^{-18}	4881
1436	0.69	1.2 × 10^{-18}	4813
2815	144.00	3.9 × 10^{-21}	30
3040	2.30	2.6 × 10^{-19}	2157
3067	1.10	5.5 × 10^{-19}	4591
3067	4.70	1.3 × 10^{-19}	1075
	$C_6H_6^{2+}$ Generated from 1,3-Cyclohexadiene		
2979	9.96	5.9 × 10^{-20}	478
3031	3.36	1.8 × 10^{-19}	1468
3073	3.24	1.9 × 10^{-19}	1565
3089	2.34	2.6 × 10^{-19}	2189
3105	4.32	1.4 × 10^{-19}	1198

[a]See the fitting curves in Figures 3 and 7 and eq 3. [b]The absolute errors of the cross sections are −30% and +50% as explained in the Supporting Information. The relative errors will be much smaller.

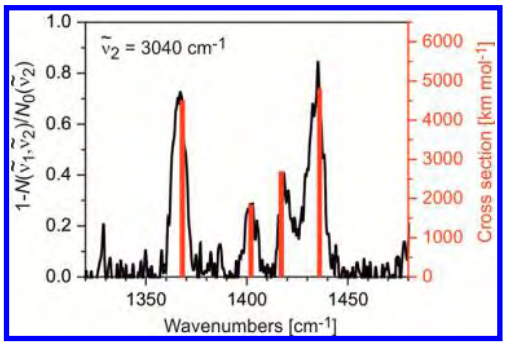

Figure 8. Comparison of the two-color IRPD spectrum for the $C_6H_6^{2+}$ dications with one OPO fixed at $\tilde{\nu}_2$ = 3040 cm^{-1} with absorption cross sections determined from the attenuation experiments.

dx.doi.org/10.1021/jp5088064 | J. Phys. Chem. A 2015, 119, 2532−2542

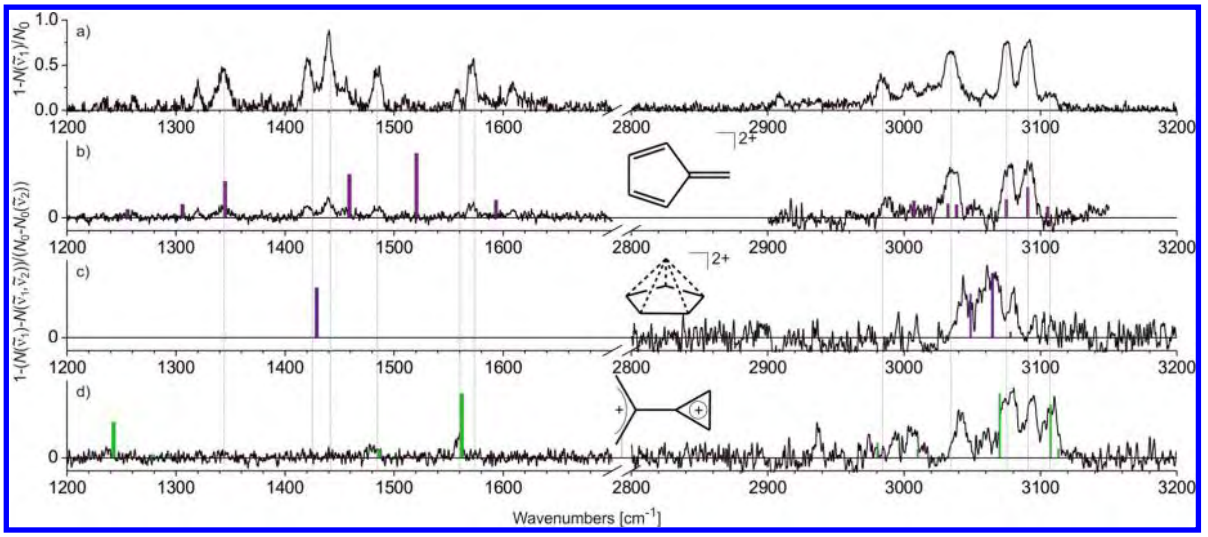

Figure 9. (a) IRPD spectrum of helium tagged $C_6H_6^{2+}$ dications generated by dissociative electron ionization from 1,3-cyclohexadiene. Two-color IRPD spectra obtained according to eq 5 with one OPO fixed at (b) 2981 cm^{-1}, (c) 3057 cm^{-1}, and (d) 3107 cm^{-1}. The bar spectra indicate theoretical IR transitions of the $C_6H_6^{2+}$ isomers (the spectra above and below 2000 cm^{-1} are normalized to 1; correct intensities can be found in Figure 4).

IRPD spectrum, because for most of the peaks more than one isomer of the generated $C_6H_6^{2+}$ dications absorb. The most representative separated spectra using the separation procedure according to eq 5 were obtained when we tuned the fixed OPO to 2981 cm^{-1} (Figure 9b), 3057 cm^{-1} (Figure 9c), and 3107 cm^{-1} (Figure 9d).

The spectrum shown in Figure 9b represents the dominant isomer. On the basis of comparison with the theoretical IR spectra, we have concluded that it corresponds to the isomer $^1\mathbf{5}^{2+}$. The theoretical IR spectrum of $^1\mathbf{5}^{2+}$ fits very well in the C−H stretching region. It, however, does not correspond well in the fingerprint region. We have optimized a whole array of other $C_6H_6^{2+}$ isomers, but there was no better match. For the fingerprint region, it could also be assumed that this isomer corresponds to $^1\mathbf{4}^{2+}$, but then the agreement in the C−H stretching region is poor. At the MP2 level of theory, the agreement between the experimental spectrum and the IR spectrum of $^1\mathbf{5}^{2+}$ is much better (cf. Figure S4 in the Supporting Information).

Irradiation with the fixed OPO at 3057 cm^{-1} led to the separation of the spectrum for a second generated isomer (Figure 9c). This is analogous to the spectrum of the pyramidal dication $^1\mathbf{2}^{2+}$ generated from benzene. The spectrum of the last isomer was obtained by setting the fixed OPO to 3107 cm^{-1} (Figure 9d). The separated spectrum probably still contains peaks from the first isomer, because it also had a low intensity absorption band at about 3107 cm^{-1}. Nevertheless, the increased intensities at 3075 and 3110 cm^{-1} together with the separated spectrum in the fingerprint region suggest that the last isomer could correspond to the $^1\mathbf{3}^{2+}$ isomer.

CONCLUSIONS

We have presented two experimental methods for disentangling isomeric mixtures of helium complexes in our cryogenic ion trap. The first one became possible by the quadrupolar field of the trap leading to an almost complete overlap between the ion cloud and the rather narrow photon beam. Up to 99% of the He-tagged ions could be fragmented with a single light pulse. This unique feature allows us to directly measure IR absorption cross sections of different helium complexes, or more precisely, cross sections for breaking the van der Waals bonds via IR excitations. In addition, the composition of isomeric mixtures can be determined by separate attenuation via their distinct absorption bands. The second possibility is based on the use of two independent IR OPOs. One of them removes a certain number of complexes whereas the other records an IRPD spectrum of the remaining He-tagged ions. In the present work the two laser like beams have been overlapped in space but separated in time by 1 ms. Nonetheless, the high power density has led to some nonlinear effects, most probably near resonant Raman heating of van der Waals modes. More work is needed to understand such effects. Additional interesting processes can be expected, if the two light pulses are synchronized.

This approach was demonstrated for highly reactive hydrocarbon dications $C_6H_6^{2+}$. We have shown that upon generation of the $C_6H_6^{2+}$ dications from different neutral precursors, completely different mixtures of isomeric dications are formed. As reported previously, the $C_6H_6^{2+}$ dications generated from benzene represent a mixture of six-membered ring isomers $^1\mathbf{1}^{2+}$ and pyramidal isomers $^1\mathbf{2}^{2+}$. We found that under the conditions of our experiment, we generated them in a 1:1 ratio. If the same dications are generated from 1,3-cyclohexadiene by dissociative electron ionization, the major component of the $C_6H_6^{2+}$ dications corresponds to the *exo*-methylenecyclopentadiene dication $^1\mathbf{5}^{2+}$. In addition, we have detected small populations of the pyramidal dication $^1\mathbf{2}^{2+}$ and the allylidenecyclopropene dication $^1\mathbf{3}^{2+}$.

ASSOCIATED CONTENT

Supporting Information

Details about determination of absorption cross sections, overlap between the photon beam and the ion cloud (Figure S1), energy per light pulse (Figure S2), two-color IRPD spectrum (Figure S3), and theoretical IR spectra obtained with the MP2 and M06-2X methods (Figures S4 and S5). This material is available free of charge via the Internet at http://pubs.acs.org.

AUTHOR INFORMATION

Corresponding Author

*J. Roithová. Phone: (420) 221951322. E-mail: roithova@natur.cuni.cz.

Notes

The authors declare no competing financial interest.

ACKNOWLEDGMENTS

The authors gratefully acknowledge financial support from the European Research Council (StG ISORI, No. 258299).

REFERENCES

(1) Kuck, D. Half a Century of Scrambling in Organic Ions: Complete, Incomplete, Progressive and Composite Atom Interchange. *Int. J. Mass Spectrom.* **2002**, *213*, 101−144.

(2) Zins, E. L.; Schröder, D. Influence of the Structure of Medium-Sized Aromatic Precursors on the Reactivity of Their Dications Towards Rare Gases. *Int. J. Mass Spectrom.* **2011**, *299*, 53−58.

(3) Roithová, J.; Schröder, D.; Schwarz, H. Substituent Effects in the Unimolecular Fragmentation of Anisole Dication Derivatives. *J. Phys. Chem. A* **2004**, *108*, 5060−5068.

(4) Knippenberg, S.; Hajgato, B.; Francois, J. P.; Deleuze, M. S. Theoretical Study of the Fragmentation Pathways of Norbornane in its Doubly Ionized Ground State. *J. Phys. Chem. A* **2007**, *111*, 10834−10848.

(5) Vachelová, J.; Roithová, J. Reactivity of $C_9H_n^{2+}$ Dications with Methane. *Int. J. Mass Spectrom.* **2012**, *311*, 51−55.

(6) Ducháčková, L.; Jašík, J.; Žabka, J.; Ascenzi, D.; Zins, E. L.; Schröder, D.; Price, S.; Alcaraz, C.; Roithová, J. Energetics and Rearrangements of the Isomeric Picoline Dications. *Int. J. Mass Spectrom.* **2011**, *308*, 81−88.

(7) Milko, P.; Roithová, J.; Schröder, D.; Schwarz, H. Doubly Protonated 1,3,5-Trimethylenebenzene ($C_9H_{11}^{2+}$) and Homologous $C_7H_7^{2+}$ and $C_8H_9^{2+}$ Dications: Structures and Unimolecular Fragmentation Patterns. *Int. J. Mass Spectrom.* **2007**, *267*, 139−147.

(8) Roithová, J.; Schröder, D.; Gruene, P.; Weiske, T.; Schwarz, H. Structural Aspects of Long-Lived $C_7H_8^{2+}$ Dications Generated by the Electron Ionization of Toluene. *J. Phys. Chem. A* **2006**, *110*, 2970−2978.

(9) Roithová, J.; Ricketts, Cl; Schröder, D. Reactions of the Dications $C_7H_6^{2+}$, $C_7H_7^{2+}$, and $C_7H_8^{2+}$ with Methane: Predominance of Doubly Charged Intermediates. *Int. J. Mass Spectrom.* **2009**, *280*, 32−37.

(10) Ricketts, Cl; Schroder, D.; Alcaraz, C.; Roithova, J. Growth of Larger Hydrocarbons in the Ionosphere of Titan. *Chem.—Eur. J.* **2008**, *14*, 4779−4783.

(11) Shaffer, C. J.; Schröder, D.; Alcaraz, C.; Žabka, J.; Zins, E. L. Reactions of Doubly Ionized Benzene with Nitrogen and Water: A Nitrogen-Mediated Entry into Superacid Chemistry. *ChemPhysChem* **2012**, *13*, 2688−2698.

(12) Duncan, M. A. Frontiers in the Spectroscopy of Mass-Selected Molecular Ions. *Int. J. Mass Spectrom.* **2000**, *200*, 545−569 and references therein..

(13) Jiang, L.; Wende, T.; Bergmann, R.; Meijer, G.; Asmis, K. R. Gas-Phase Vibrational Spectroscopy of Microhydrated Magnesium Nitrate Ions $[MgNO_3(H_2O)_{1-4}]^+$. *J. Am. Chem. Soc.* **2010**, *132*, 7398−7404.

(14) Goebbert, D. J.; Wende, T.; Bergmann, R.; Meijer, G.; Asmis, K. R. Messenger-Tagging Electrosprayed Ions: Vibrational Spectroscopy of Suberate Dianions. *J. Phys. Chem. A* **2009**, *113*, 5874−5880.

(15) Okumura, M.; Yeh, L. I.; Myers, J. D.; Lee, Y. T. Infrared Spectra of the Solvated Hydronium Ion: Vibrational Predissociation Spectroscopy of Mass-Selected $H_3O^+\cdot(H_2O)_n\cdot(H_2)_m$. *J. Phys. Chem.* **1990**, *94*, 3416−3457.

(16) Coker, D. F.; Miller, R. E.; Watts, R. O. The Infrared Predissociation Spectra of Water Clusters. *J. Chem. Phys.* **1985**, *82*, 3554.

(17) Walker, N. R.; Walters, R. S.; Duncan, M. A. Frontiers in the Infrared Spectroscopy of Gas Phase Metal Ion Complexes. *New J. Chem.* **2005**, *29*, 1495−1503.

(18) Carnegie, P. D.; Bandyopadhyay, B.; Duncan, M. A. Infrared Spectroscopy of $Sc^+(H_2O)$ and $Sc^{2+}(H_2O)$ via Argon Complex Predissociation: The Charge Dependence of Cation Hydration. *J. Chem. Phys.* **2011**, *134*, 014302.

(19) Duncan, M. A. Infrared Laser Spectroscopy of Mass-Selected Carbocations. *J. Phys. Chem. A* **2012**, *116*, 11477−11491.

(20) Ascenzi, D.; Tosi, P.; Roithová, J.; Ricketts, C. L.; Schröder, D.; Lockyear, J. F.; Parkes, M. A.; Price, S. D. Generation of the Organo-Rare Gas Dications $HCCRg^{2+}$ (Rg = Ar and Kr) in the Reaction of Acetylene Dications with Rare Gases. *Phys. Chem. Chem. Phys.* **2008**, *10*, 7121−7128.

(21) Roithova, J.; Schroder, D. Silicon Compounds of Neon and Argon. *Angew. Chem., Int. Ed.* **2009**, *48*, 8788−8790.

(22) Khriachtchev, L.; Pettersson, M.; Runeberg, N.; Lundell, J.; Rasanen, M. A Stable Argon Compound. *Nature* **2000**, *406*, 874−876.

(23) Pettersson, M.; Lundell, J.; Rasanen, M. New Rare-Gas-Containing Neutral Molecules. *Eur. J. Inorg. Chem.* **1999**, 729−737.

(24) Khriachtchev, L.; Rasanen, M.; Gerber, R. B. Noble-Gas Hydrides: New Chemistry at Low Temperatures. *Acc. Chem. Res.* **2009**, *42*, 183−191.

(25) Jašík, J.; Žabka, J.; Roithová, J.; Gerlich, D. Infrared Spectroscopy of Trapped Molecular Dications Below 4 K. *Int. J. Mass Spectrom.* **2013**, *354*−*355*, 204−210.

(26) Johnson, C. J.; Wolk, A. B.; Fournier, J. A.; Sullivan, E. N.; Weddle, G. H.; Johnson, M. A. Communication: He-Tagged Vibrational Spectra of the $SarGlyH^+$ and $H^+(H_2O)_{2,3}$ Ions: Quantifying Tag Effects in Cryogenic Ion Vibrational Predissociation (CIVP) Spectroscopy. *J. Chem. Phys.* **2014**, *140*, DOI: 10.1063/1.4880475.

(27) Chakrabarty, S.; Holz, M.; Campbell, E. K.; Banerjee, A.; Gerlich, D.; Maier, J. P. A Novel Method to Measure Electronic Spectra of Cold Molecular Ions. *J. Phys. Chem. Lett.* **2013**, *4*, 4051−4054.

(28) Jašik, J.; Roithova, J. Infrared Spectroscopy of $CHCl^{2+}$ Molecular Dications. *Int. J. Mass Spectrom.* **2014**, DOI: 10.1016/j.ijms.2014.07.001.

(29) Asvany, O.; Brunken, S.; Kluge, L.; Schlemmer, S. COLTRAP: a 22-Pole Ion Trapping Machine for Spectroscopy at 4 K. *Appl. Phys. B: Lasers Opt.* **2014**, *114*, 203−211.

(30) Dietl, N.; Wende, T.; Chen, K.; Jiang, L.; Schlangen, M.; Zhang, X. H.; Asmis, K. R.; Schwarz, H. Structure and Chemistry of the Heteronuclear Oxo-Cluster $[VPO_4]^{\bullet+}$: A Model System for the Gas-Phase Oxidation of Small Hydrocarbons. *J. Am. Chem. Soc.* **2013**, *135*, 3711−3721.

(31) Jašík, J.; Gerlich, D.; Roithová, J. Probing Isomers of the Benzene Dication in a Low-Temperature Trap. *J. Am. Chem. Soc.* **2014**, *136*, 2960−2962.

(32) Krogh-Jespersen, K. Ab Initio Electronic Structure Calculations on the Benzene Dication and Other $C_6H_6^{2+}$ Isomers. *J. Am. Chem. Soc.* **1991**, *113*, 417−423.

(33) Gerlich, D. In *Low Temperatures and Cold Molecules*; Smith, I. W. M., Ed.; Imperial College Press, distributed by World Scientific Publishing Co. Pte. Ltd.: Singapore, 2008; pp 295 − 343.

(34) Wolk, A. B.; Leavitt, C. M.; Garand, E.; Johnson, M. A. Cryogenic Ion Chemistry and Spectroscopy. *Acc. Chem. Res.* **2014**, *47*, 202−210.

(35) Ducháčková, L.; Roithová, J. The Interaction of Zinc(II) and Hydroxamic Acids and a Metal-Triggered Lossen Rearrangement. *Chem.—Eur. J.* **2009**, *15*, 13399−13405.

(36) Ricks, A. M.; Douberly, G. E.; Schleyer, P. v. R.; Duncan, M. A. Communications: Infrared Spectroscopy of Gas Phase $C_3H_3^+$ Ions: The Cyclopropenyl and Propargyl Cations. *J. Chem. Phys.* **2010**, *132*, 051101−1−051101−4.

(37) Douberly, G. E.; Ricks, A. M.; Schleyer, P. v. R.; Duncan, M. A. Infrared Spectroscopy of Gas Phase $C_3H_5^+$: The Allyl and 2-Propenyl Cations. *J. Chem. Phys.* **2008**, *128*, 021102.

(38) Ebata, T.; Watanabe, T.; Mikami, N. Evidence for the Cyclic Form of Phenol Trimer: Vibrational Spectroscopy of the OH Stretching Vibrations of Jet-Cooled Phenol Dimer and Trimer. *J. Phys. Chem.* **1995**, *99*, 5761−5764.
(39) Nagornova, N. S.; Rizzo, T. R.; Boyarkin, O. V. Exploring the Mechanism of IR−UV Double-Resonance for Quantitative Spectroscopy of Protonated Polypeptides and Proteins. *Angew. Chem., Int. Ed.* **2013**, *52*, 6002−6005.
(40) Møller, C.; Plesset, M. S. Note on an Approximation Treatment for Many-Electron Systems. *Phys. Rev.* **1934**, *46*, 618−622.
(41) Frisch, M. J.; Head-Gordon, M.; Pople, J. A. Direct MP2 Gradient Method. *Chem. Phys. Lett.* **1990**, *166*, 275−280.
(42) Frisch, M. J.; Head-Gordon, M.; Pople, J. A. Semi-Direct Algorithms for the MP2 Energy and Gradient. *Chem. Phys. Lett.* **1990**, *166*, 281−289.
(43) Ernzerhof, M.; Perdew, J. P. Generalized Gradient Approximation to the Angle- and System-Averaged Exchange Hole. *J. Chem. Phys.* **1998**, *109*, 3313.
(44) Perdew, J. P.; Burke, K.; Ernzerhof, M. Generalized Gradient Approximation Made Simple. *Phys. Rev. Lett.* **1996**, *77*, 3865−3868.
(45) Frisch, M. J.; Trucks, G. W.; Schlegel, H. B.; Scuseria, G. E.; Robb, M. A.; Cheeseman, J. R.; Scalmani, G.; Barone, V.; Mennucci, B.; et al. *Gaussian 09*, Revision A.02; Gaussian, Inc.: Wallingford, CT, 2009.
(46) Čížek, J. In *Advances in Chemical Physics*; Hariharan, P. C., Ed.; Wiley Interscience: New York, 1969; Vol. *14*, p 35.
(47) Purvis, G. D., III; Bartlett, R. J. A Full Coupled-Cluster Singles and Doubles Model - the Inclusion of Disconnected Triples. *J. Chem. Phys.* **1982**, *76*, 1910−1918.
(48) Scuseria, G. E.; Janssen, C. L.; Schaefer, H. F., III. An Efficient Reformulation of the Closed-Shell Coupled Cluster Single and Double Excitation (CCSD) Equations. *J. Chem. Phys.* **1988**, *89*, 7382−7387.
(49) Shubert, V. A.; Zwier, T. S. IR−IR−UV Hole-Burning: Conformation Specific IR Spectra in the Face of UV Spectral Overlap. *J. Phys. Chem. A* **2007**, *111*, 13283−13286.
(50) Elliott, B. M.; Relph, R. A.; Roscioli, J. R.; Bopp, J. C.; Gardenier, G. H.; Guasco, T. L.; Johnson, M. A. Isolating the Spectra of Cluster Ion Isomers Using Ar-"Tag"-Mediated IR−IR Double Resonance Within the Vibrational Manifolds: Application to $NO_2^-\cdot H_2O$. *J. Chem. Phys.* **2008**, *129*, 094303.
(51) Heine, N.; Fagiani, M. R.; Rossi, M.; Wende, T.; Berden, G.; Blum, V.; Asmis, K. R. Isomer-Selective Detection of Hydrogen-Bond Vibrations in the Protonated Water Hexamer. *J. Am. Chem. Soc.* **2013**, *135*, 8266−8273.
(52) Rizzo, T. R.; Stearns, J. A.; Boyarkin, O. V. Spectroscopic Studies of Cold, Gas-Phase Biomolecular Ions. *Int. Rev. Phys. Chem.* **2009**, *28*, 481−515.
(53) Best, T.; Otto, R.; Trippel, S.; Hlavenka, P.; von Zastrow, A.; Eisenbach, S.; Jezouin, S.; Wester, R.; Vigren, E.; Hamberg, M.; Geppert, W. D. Absolute Photodetachment Cross-Section Measurements for Hydrocarbon Anions. *Astrophys. J.* **2011**, *742*, 63−68.
(54) Roithová, J.; Schröder, D.; Berger, R.; Schwarz, H. Doubly Protonated Benzene in the Gas Phase. *J. Phys. Chem. A* **2006**, *110*, 1650−1657.

SUPPORTING INFORMATION

for

Two Color Infrared Predissociation Spectroscopy of $C_6H_6^{2+}$ Isomers Using Helium Tagging

Juraj Jašík,[‡] Dieter Gerlich,[‡,†] and Jana Roithová*[‡]

[‡]Department of Organic Chemistry, Faculty of Science, Charles University in Prague, Hlavova 2030/8, 12843 Prague 2, Czech Republic

[†]Department of Physics, University of Technology, 09107 Chemnitz, Germany

Content: **Page**

Ion density, light beam, fluence of photons, cross section

In order to determine absolute cross sections for absorbing one or several IR photons, it needs to be accounted for the spatial overlapping integral of the ion cloud and the laser-like OPO beam penetrating the trap. In the following we show that the ion cloud is much smaller than the focused near Gaussian light beam, allowing us to use a rather simple estimate.

The central element of the instrument ISORI is an rf (radio frequency) ion trap mounted onto a cold head. As described in detail in Ref. 25, a linear wire quadrupole (w4PT) has been chosen in the present instrument. The hyperbolic boundary conditions are approximated by four groups of 6 wires (diameter 1 mm, see left part of Figure S1). In comparison to higher order multipoles, more often used for cryogenic ion traps, this geometry has several advantages due to the harmonic effective potential, while rf heating leads to a higher kinetic temperature. However, if heavy ions are stored in He, the internal temperature of the ions is much less effected (see Eq. 113 in Ref. (S1)).

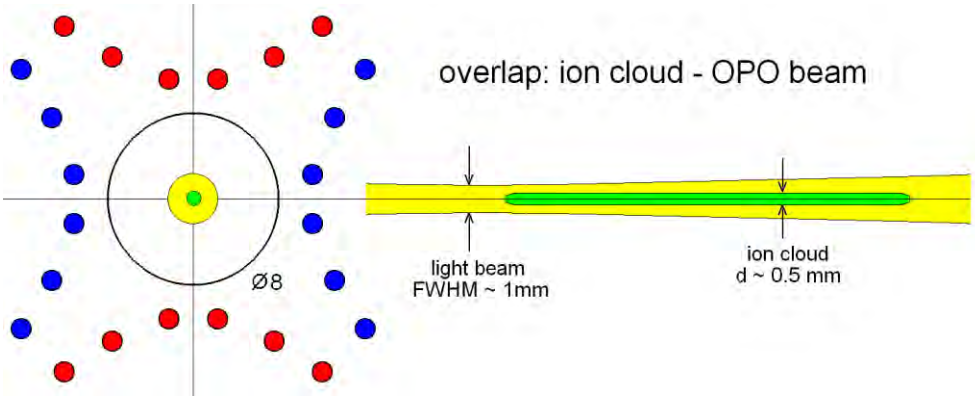

Figure S1. Overlap between the photon beam (yellow) and the ion cloud (green). The inhomogeneous rf field of the w4PT confines the ion cloud very close to the center line of the linear quadrupole. The broader laser beam surrounds the ions. The influence of space charge and a non-ideal beam profile of the OPO output are discussed in the text.

In order to estimate the spatial distribution of the ion cloud, we make use of Eq. 54 from Ref. (S1). In the present experiment the quadrupole (inscribed radius $r_0 = 0.6$ cm) is operated with a frequency $f = 3.0$ MHz and an amplitude $V_0 = 130$ V. For ions with $m/q = 41$ u/e and a kinetic energy of $E_m = 1$ meV (~ 10 K), one obtains a turning radius $r_m = 0.108$ mm. With typically 10^4 ions in the 4 cm long trapping volume, this would lead to a number density of 6.8×10^6 ions/cm^3, a value where Coulomb repulsion starts to play a role (see for example Ref. S(2)). Accounting for this and assuming a kinetic temperature of 20 K we estimate that the diameter of the ion cloud is at maximum 0.5 mm.

The beams from the two OPOs (LaserVision) are first expanded (4 : 1) and then, using a 50 % beam splitter, superimposed parallel before they enter the vacuum system. The overall distance from the entrance to the exit window is 126 cm allowing very precise alignment. The energy of each OPO pulse is monitored after the exit window. Typical results are shown in Figure S2.

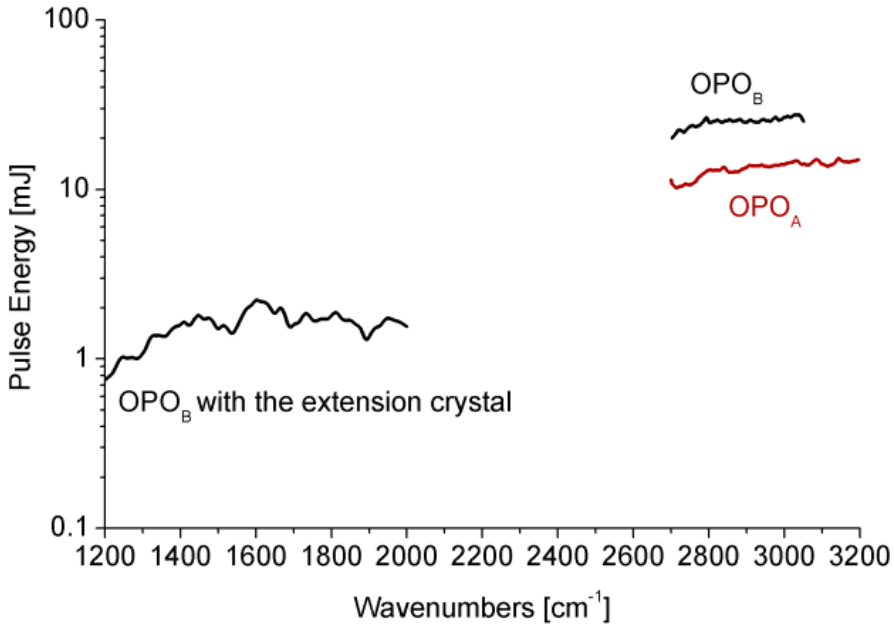

Figure S2. Energy per light pulse determined after the exit window of the instrument and corrected for the calibrated transmission trap - exit window.

Using a telescope, the trap and the cold head, which is mounted with bellows, have been adjusted onto the axis of the apparatus. A lens with an effective focal length of 65 cm focuses the light beam into the instrument such that the beam waist is located several cm before the trap. In this way a light beam with a slowly increasing diameter is superimposed to the ion cloud (see Figure S1). The beam profile at the location of the trap has been analyzed deviating the beam with a mirror before the entrance window.

Averaging over the beam profile at the location of the ions (d ~ 0.5 mm) and accounting for the slight divergence of the light beam (~ 3.5×10^{-3}) we estimate that the photon fluence Φ, seen by the ions, can be determined simply from the measured energy per pulse and an effective area $a = 1^{+0.5}_{-0.3} mm^2$. The errors account for deviations from a Gaussian profile, for slight deviations of the trap axis and also for possible field perturbations inside the trap, occurring especially at the two ends of the linear quadrupole. It is important to note that the reduction of the rf amplitude by a factor 2 (V_0 = 65 V) did not lead to a significant change of the fragmentation signal although the radius of the ion cloud is doubled. This test, which has been performed in the linear regime, indicates that the ion cloud is located in the plateau region of the light beam. It also corroborates our simplifying assumption to use simply a mean value for Φ.

With the information presented above, one can convert directly the measured pulse energy into the photon fluence Φ and the measured characteristic energies E_j (see Eq. 3) into the absorption cross section σ_j using the formulas:

$$\phi = E / a\ h\nu . \tag{S1}$$

$$\sigma_j = a\ h\nu / E_j . \tag{S2}$$

The error of the so-derived cross sections is predominantly determined by the error of the area *a*, e.g. -30% and + 50%.

Third isomer among the $C_6H_6^{2+}$ dications generated from benzene

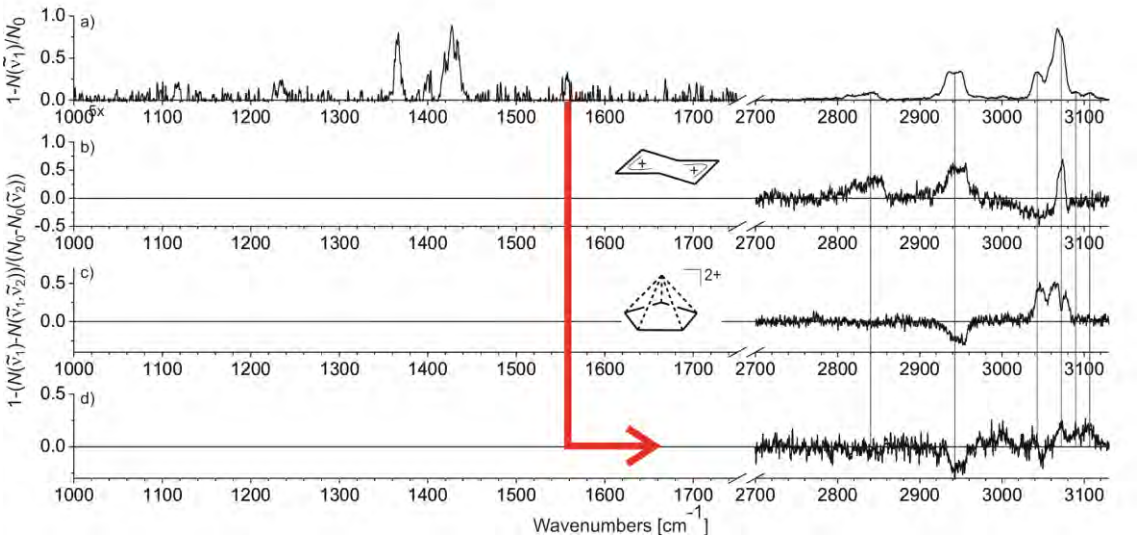

Figure S3. (a) IRPD spectrum of the helium tagged $C_6H_6^{2+}$ dications generated from benzene. double resonance IRPD spectra obtained according to Equation 1 with the fixed laser at (b) 2940 cm^{-1}, (c) 3040 cm^{-1}, and (d) 1555 cm^{-1}.

The bands at 1555 cm^{-1} and 1233 cm^{-1} did not appear during all measurements. It could be due to a third type of isomers among the $C_6H_6^{2+}$ dications generated from benzene that are formed with a low population and their formation depends on the conditions in the ion source. Double resonance IRPD spectrum that was measured for this particular isomer by fixing one laser at 1555 cm^{-1} and scanning the C-H stretching mode region reveals that it could be one of the isomers generated from 1,3-cyclohexadiene (cf. Figure 9d in the main document). This isomer is probably allylidenecyclopropene dication $^1\mathbf{3}^{2+}$.

Theoretical spectra calculated at different levels of theory

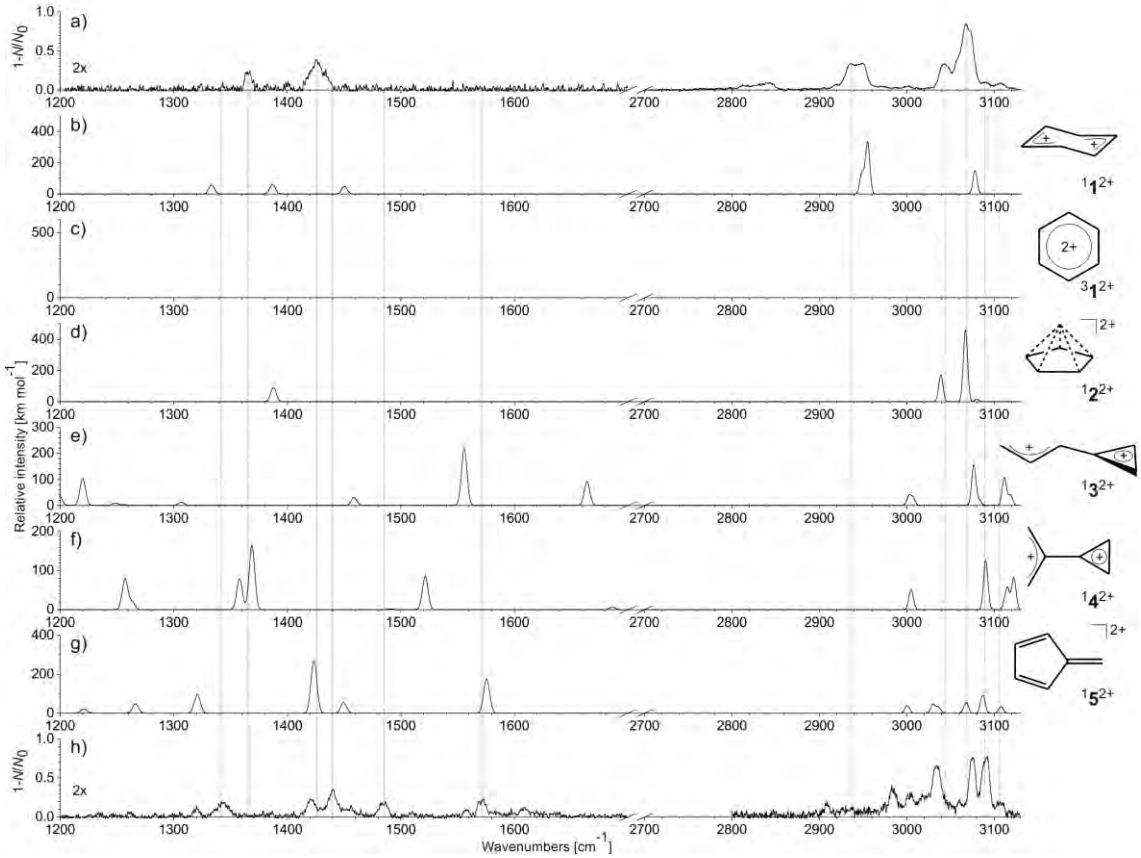

Figure S4. Helium tagging IRPD spectra of the $C_6H_6^{2+}$ dications generated by (a) double ionization of benzene and (h) dissociative double ionization of 1,3-cyclohexadiene. Note that the spectra in the finger-print region are twice enhanced. (b-g) Theoretical IR spectra of different $C_6H_6^{2+}$ isomers obtained with perturbation theory MP2; scaling factor was 0.955 for the whole spectra.

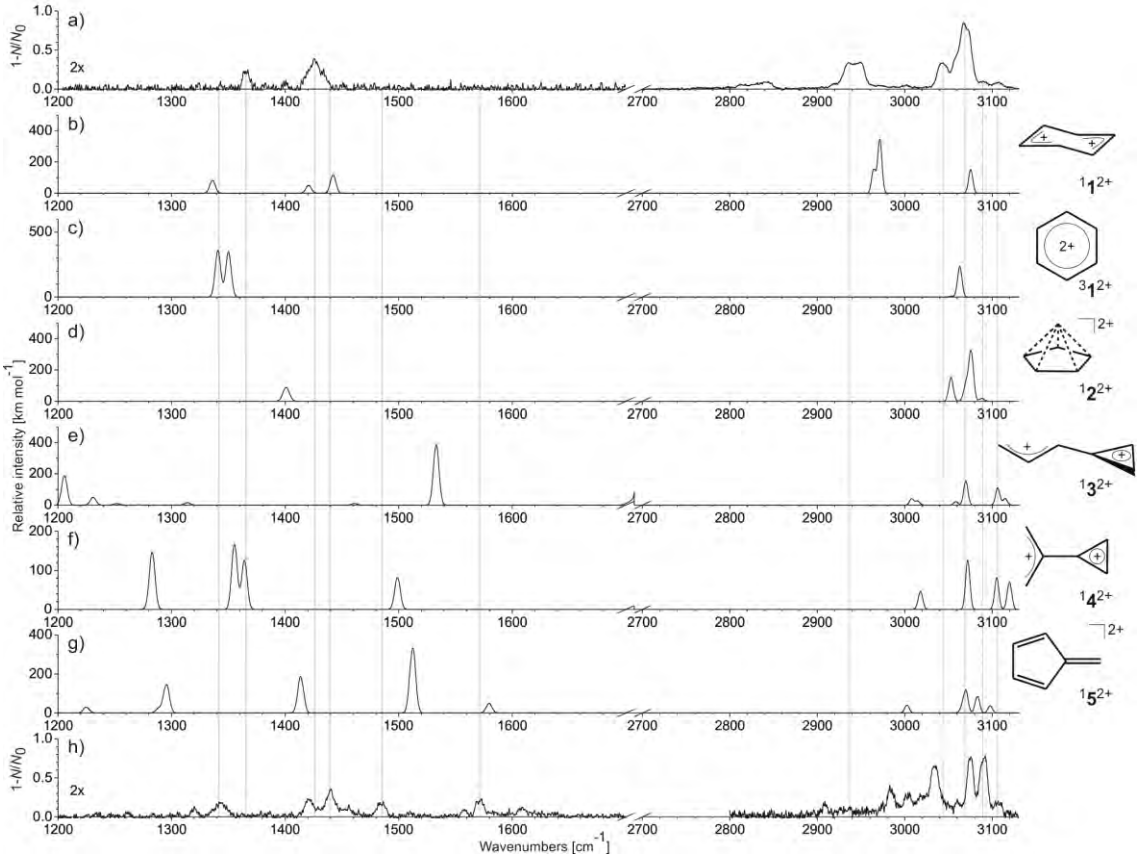

Figure S5. Helium tagging IRPD spectra of the $C_6H_6^{2+}$ dications generated by (a) double ionization of benzene and (h) dissociative double ionization of 1,3-cyclohexadiene. Note that the spectra in the finger-print region are twice enhanced. (b-g) Theoretical IR spectra of different $C_6H_6^{2+}$ isomers obtained with density functional theory M06-2X; scaling factor was 0.955 for the whole spectra.

References

(S1) Gerlich, D. Inhomogeneous Electrical Radio Frequency Fields: A Versatile Tool for the Study of Processes with Slow Ions, in: State-Selected and State-to-State Ion-Molecule Reaction Dynamics, edited by C.Y.Ng and M. Baer. Advances in Chemical Physics Series, LXXXII, 1 – 176, J. Wiley & Sons (1992)

(S2) Gerlich, D.; Decker, S. Trapping Ions at High Temperatures: Thermal Decay of C_{60}^+, *Appl. Phys. B* **2014**, *114*, 257 – 266.